New Journal of Physics
The open access journal at the forefront of physics

Deutsche Physikalische Gesellschaft DPG IOP Institute of Physics

PAPER • OPEN ACCESS

Evaluation of photocathode emission properties in an electron gun: one-step photoemission from bulk band to vacuum states

To cite this article: W Andreas Schroeder and Gowri Adhikari 2019 *New J. Phys.* **21** 033040

New Journal of Physics
The open access journal at the forefront of physics

Deutsche Physikalische Gesellschaft DPG
IOP Institute of Physics

Published in partnership with: Deutsche Physikalische Gesellschaft and the Institute of Physics

CrossMark

OPEN ACCESS

RECEIVED
12 October 2018

REVISED
14 January 2019

ACCEPTED FOR PUBLICATION
5 March 2019

PUBLISHED
29 March 2019

PAPER

Evaluation of photocathode emission properties in an electron gun: one-step photoemission from bulk band to vacuum states

W Andreas Schroeder and Gowri Adhikari

University of Illinois at Chicago, Department of Physics (m/c 273), 845 W Taylor Street, Chicago, IL 60607-7059, United States of America

E-mail: andreas@uic.edu

Keywords: vacuum density of states, photoemission, photocathode physics

Abstract

A one-step photoemission analysis is developed, using the exact one-dimensional quantum solution for transmission over and through a triangular barrier presented by Forbes and Deane (2011 *Proc. R. Soc. A* **467** 2927), to evaluate the emission properties of a photocathode in an electron gun. The analysis, which employs transverse momentum conservation in electron emission, includes the physical attributes (density of states and energy-momentum dispersion) of both the bulk band emission states and the recipient vacuum states in its evaluation of the mean transverse energy and relative quantum efficiency of the emitted electrons.

1. Introduction

Planar, pulsed laser-driven, solid-state photocathodes are the most commonly employed electron sources for of x-ray free electron lasers (XFELs) [1, 2], ultrafast electron diffraction [3–6] systems, and current (and potential future ultrafast) dynamic transmission electron microscopes (DTEMs) [7–9]—cutting-edge research instruments designed to study the atomic-scale dynamic properties of matter on fast timescales. The space-time resolution performance of these instruments is known to be limited primarily by the emission properties of the cathode. Of particular importance is the normalized emittance of photocathodes or, equivalently, the mean transverse energy (MTE) of the emitted electrons [10, 11] as this determines the spatial divergence of the electron beam and hence its focusability (or beam quality). A lower emittance (or MTE) will provide for higher quality and higher photon energy x-ray beams generated by XFELs [12, 13], improved fidelity of electron diffraction patterns through increased spatial beam coherence [6, 14], and higher spatial resolution in DTEMs through a reduction in the focal spot size.

Prior theoretical analyses have connected the MTE from planar photocathodes to both the maximum excess energy of photoemission [15, 16], $\Delta E = \hbar\omega - \phi$ (where $\hbar\omega$ is the incident photon energy and ϕ is the work function), and the photocathode temperature [17], specifically the temperature T_e of the electrons, through the inclusion of the Fermi–Dirac distribution. More recent work [18–21] has indicated that the bulk electronic states from which the electron originate also need to be included as their band dispersion (i.e. effective mass, m^*) and density of states variation affects, and can limit, the MTE of the emitted electrons through transverse momentum conservation in photoemission [22]. Together with the work function variation with crystal orientation [23], this is now leading to experimental investigations of the spectral emission properties of single-crystal photocathodes [24–27] for which a functional theory [28] is required to aid our understanding of photoemission and, consequently, the selection of future high brightness (low MTE and high quantum efficiency (QE)) photocathode materials.

In this paper, we present a new theoretical formulation of one-step photoemission [29] based on the exact one-dimensional quantum solution for transmission through ($\Delta E < 0$) and over ($\Delta E > 0$) a triangular barrier evaluated by Forbes and Deane [30]. The exact quantum solution is extended into the transverse dimension, using conservation of transverse momentum in electron emission [22], to include a parabolic bulk electronic band associated with a 'perfect' metal; that is, an emission band with spherical symmetry and an electron mass equal to the free electron mass m_0. In addition to incorporating the local density of the emitting states

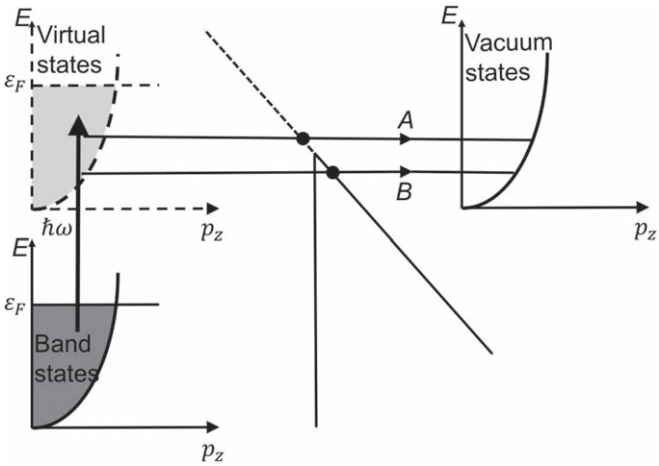

Figure 1. Schematic of the simulated one-step photoemission process: photo-excitation of the bulk band states into a set of identical virtual band states from which electrons transmit (with transverse momentum conservation) into the vacuum states either above (photoemission with $\Delta E > 0$; path (A)) or below (photo-assisted tunneling with $\Delta E < 0$; path (B)) the triangular barrier generated by the applied acceleration field in an electron gun: $\varepsilon_F =$ Fermi energy.

(multiplied by the appropriate Fermi–Dirac population distribution) in the photoemission simulation, we have also now included the vacuum density of states; that is, the density of the recipient states for the emitted electron. This hither-to-fore omitted (to our knowledge) latter factor has a significant effect on both the MTE of the electron distribution emitted from photocathodes and the QE of photoemission.

2. Photoemission formalism

The essential features of the presented one-step photoemission analysis are schematically illustrated in figure 1. The bulk electronic band states are photo-excited by the incident photon energy $\hbar\omega$ to form a set of 'virtual' electronic states whose energy-momentum dispersion relation is, to a very good approximation, a replica (at the higher energy) of that of the bulk band states since the photon momentum is much less than the electron momenta in the band [18]. These excited states, if occupied in the bulk, may emit electrons into the vacuum under the necessary energy-momentum conservation by either above barrier photoemission or photo-assisted tunneling; respectively, paths A and B in figure 1. The transmission through or over the triangular barrier generated by an applied surface acceleration field E_{acc} of the electron gun is described by Forbes and Deane's recent exact analytical one-dimensional quantum solution [30]. In our extension of this formalism into the transverse dimension parallel to the planar photocathode surface, we invoke transverse momentum conservation in the electron emission [22], employ the energy-momentum relationships of both the bulk and vacuum states, and include their local density of states (LDS). Consequently, at each transverse momentum p_T associated with a bulk band energy E, the one-step simulation evaluates the product of the emitting bulk band LDS, their occupation (using a Fermi–Dirac population distribution), the transmission coefficient of the triangular barrier, and the local density of the available vacuum state into which the emitting electron is to be received. The inclusion of the latter implies that the 'joint density of states' between the initial occupied and final unoccupied states is evaluated explicitly as is required in any description of band-to-band transitions; for example, optical absorption in semiconductors [31].

For simplicity, our simulation of one-step photoemission assumes that the emission is from a positive dispersion and bulk electron band with an effective mass equal to the free electron mass m_0 in the first Brillouin zone; that is, an energy-momentum relation of the form

$$E(\mathbf{p}) = \frac{p_z^2 + p_T^2}{2m_0}, \tag{1}$$

where p_z is the longitudinal electron momentum in the band. The LDS of such an isotropic band is proportional to $m_0^{3/2}\sqrt{E} = m_0\sqrt{(p_z^2 + p_T^2)/2}$, and the occupation of the band at any energy E is a function of both the Fermi energy ε_F and the electron temperature T_{e} through the Fermi–Dirac distribution;

$$f(E) = \frac{1}{(1 + \exp[(E - \varepsilon_F)/k_{\mathrm{B}}T_{\mathrm{e}}])}, \tag{2}$$

where k_B is Boltzmann's constant. Equation (1) defines the longitudinal kinetic energy of the electron in the band as $K_z = E(\mathbf{p}) - \frac{p_T^2}{2m_T}$ which then allows the bulk band dispersion to be included in the transmission coefficient of the triangular barrier for emitted electrons [30];

$$T = \frac{4Cp_z}{(2Cp_z + \pi C^2 p_z^2(\mathrm{Ai}^2(\xi) + \mathrm{Bi}^2(\xi)) + \pi((\mathrm{Ai}'(\xi))^2 + (\mathrm{Bi}'(\xi))^2))}, \tag{3}$$

where $C = (2m_0\hbar e E_{\mathrm{acc}})^{-1/3}$ with e the free electron charge and $\hbar$ Planck's constant divided by 2π, and $\mathrm{Ai}(\xi)$ and $\mathrm{Bi}(\xi)$ are Airy functions of the first and second kind, respectively, with the prime denoting the first derivative. The Airy function argument is given by

$$\xi = \sqrt[3]{\frac{2m_0}{(\hbar e E_{\mathrm{acc}})^2}}(E_{\mathrm{th}} - K_z), \tag{4}$$

where the bulk band threshold energy for above barrier photoemission $E_{\mathrm{th}} = \varepsilon_F - \Delta E$. Finally, the density of the recipient vacuum state for the emitted electron at the conserved value of the transverse momentum is proportional to $m_0\sqrt{p_{z0}^2 + p_T^2}$, where p_{z0} is the longitudinal momentum in the vacuum at emission. The exact analytical solution of Forbes and Deane [30] also allows for the evaluation of p_{z0} for emission above and below the barrier;

$$p_{z0}(\mathrm{above}) = \frac{1}{C}\left|\frac{\mathrm{Ai}'(\xi) - \mathrm{iBi}'(\xi)}{\mathrm{Ai}(\xi) - \mathrm{iBi}(\xi)}\right| \tag{5a}$$

and

$$p_{z0}(\mathrm{below}) = \frac{1}{C}\left|\frac{\mathrm{Ai}'(0) - \mathrm{iBi}'(0)}{\mathrm{Ai}(0) - \mathrm{iBi}(0)}\right|. \tag{5b}$$

We note here that equation (5*a*) is entirely consistent with the expectation that the maximum value of p_{z0} is equal to $\sqrt{2m_0(\hbar\omega - \phi)}$ when $T_e \to 0$. Further, equation (5*b*) indicates that p_{z0} below the barrier is small but not equal to zero unless $E_{\mathrm{acc}} = 0$, in which case below barrier transmission ceases.

The presented one-step photoemission simulation uses the above to evaluate the relative number of electrons emitted at each value of the transverse momentum by summing over all energy states contributing to emission at that value of p_T. The MTE is then obtained by taking the normalized second order moment of the evaluated transverse momentum distribution of the emitted electrons in the vacuum, $MTE = \langle p_T^2\rangle / m_0$, and the QE (in arbitrary units) is calculated by simply integrating over the distribution.

In figure 2, as a comparative example, the result of evaluating both the MTE and QE as a function of excess energy ΔE for a Ag(100) photocathode are presented; for which the work function $\phi = 4.36$ eV [23], the effective mass m^* of the emitting electrons near the Fermi level in the bulk band is (to a good approximation) equal to m_0 [32], and the Fermi energy $\varepsilon_F = 5.49$ eV. Room temperature operation ($T_e = 300$ K) is assumed and we employ a surface acceleration field of 1 MV m^{-1} typical of a DC electron gun for the simulation. The evaluation of the MTE using our one-step photoemission simulation (black solid line) is compared in figure 2(a) with the results of two prior analyses; the formulation of Dowell and Schmerge [15] for which MTE $= \Delta E/3$ (dashed red line), and the more recent expression derived by Vecchione *et al* [17] (red solid line)

$$\mathrm{MTE} = k_B T_e\left\{\frac{\mathrm{Li}_3\left[-\mathrm{Exp}\left(\frac{\Delta E}{k_B T_e}\right)\right]}{\mathrm{Li}_2\left[-\mathrm{Exp}\left(\frac{\Delta E}{k_B T_e}\right)\right]}\right\}, \tag{6}$$

where Li_n is the ploy-logarithm function of order n. The latter, which asymptotically tends to the result of Dowell and Schmerge [15] at high excess energies, underestimates the MTE at all ΔE since it does not include either the bulk band or vacuum states. The expression of equation (6) does however agree with our one-step model below the photoemission threshold ($\Delta E < 0$) when the vacuum density of states are omitted in the simulation (black dashed line)—both giving a limiting value $k_B T_e \approx 25$ meV for the MTE, as is also the case for the extension of the Dowell and Schmerge theory presented in [20]. This is because the electrons emitting from the population in the thermal Boltzmann tail that extends above the photoemission barrier have a sufficiently small energy spread $\sim k_B T_e$ to ensure that they originate from a relatively constant density of states in the bulk band—the approximation employed in obtaining equation (6). Consequently, the increase in the MTE to 31.5($\pm$0.5) meV when $\Delta E < 0$ evaluated with the full one-step simulation is entirely due to the increase with higher electron momenta of the recipient vacuum density of states. As ΔE increases above threshold, both one-step simulations with and without the vacuum states return higher values of the MTE than that predicted by the prior analyses [15, 17] due to the inclusion of the bulk band states. For excess energies greater than 0.1 eV, our full one-step

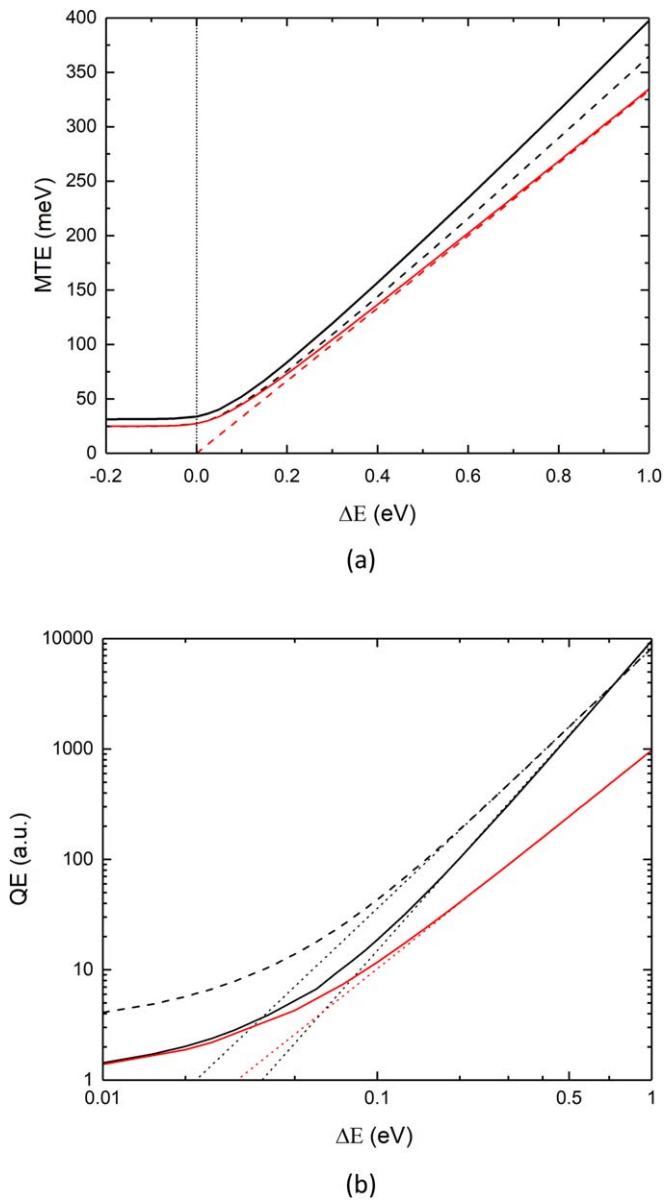

Figure 2. Emission properties of a Ag(100) photocathode at 300 K ($\phi = 4.36$ eV, bulk electron mass $= m_0$, ε_F=5.49 eV, and $E_{\text{acc.}} = 1$ MV m^{-1}): (a) MTE as a function of the excess photoemission energy ΔE; full one-step simulation (black line), one-step simulation without the vacuum states (black dashed line), equation (6) (red line) [17], and $\Delta E/3$ (red dashed line) [15]. (b) QE as a function of ΔE; full one-step simulation (black line), one-step simulation without the vacuum states (black dashed line), and equation (7) (red line) [17], with corresponding power law fits for $\Delta E > 0.25$ eV shown as thin dotted lines.

photoemission model predicts MTE values 15%–20% greater than obtained from equation (6) for the simulated Ag(100) photocathode. We note that photo-assisted tunneling (below barrier emission) is negligible in this example, contributing less than 1% of the emitted electrons even at $\Delta E = -0.2$ eV for the employed 1 MV m^{-1} acceleration field, and so does not contribute significantly to the presented MTE results.

The simulated spectral dependence of the QE for the Ag(100) photocathode example is shown in figure 2(b) (black line) together with the QE dependence predicted by Vecchione *et al* [17] (red line);

$$\text{QE} = S_{12}\left\{\frac{\text{Li}_2\left[-\text{Exp}\left(\frac{\Delta E}{k_\text{B}T_\text{e}}\right)\right]}{\text{Li}_2\left[-\text{Exp}\left(\frac{E_F}{k_\text{B}T_\text{e}}\right)\right]}\right\}, \tag{7}$$

where S_{12} is a constant associated with the matrix element of optical excitation, transmission into the vacuum, etc. For the purpose of comparison, both our simulated one-step photoemission data and the dependence described by equation (7) are normalized to unity at $\Delta E = 0$. Both our one-step model and equation (7) display the expected rapid increase of the QE with ΔE associated with the strongly increasing number of filled bulk band

states that can emit electrons into the vacuum as the excess energy increases. However, the log–log plot of figure 2(b) clearly indicates that the one-step simulation predicts a different power law dependence for the QE on ΔE than equation (7) for excess energies greater than 0.25 eV $= 10k_{\mathrm{B}}T_{\mathrm{e}}$. A fit (dotted line) to our one-step simulation for this Ag(100) example indicates that QE $= A(\Delta E)^{2.85}$, where A is a constant, whereas equation (7) returns the Fowler–DuBridge relation of a quadratic power law dependence (red dotted line); i.e. QE $= A(\Delta E)^2$ [33, 34]. The difference in these power law dependences is directly related to the inclusion of the bulk band and vacuum states in our one-step simulation, both of which are omitted in prior analyses [15, 17, 33, 34]. Indeed, removal of the vacuum density of states from the one-step analysis generates the data set shown by the black dashed line in figure 2(b) for which the dependence on excess energy is of the form QE $= A(\Delta E)^{2.4}$ for $\Delta E > 10k_{\mathrm{B}}T_{\mathrm{e}}$ (dotted line)—a power law dependence between that of equation (7) and our full one-step photoemission simulation. This latter data set is normalized by the QE with the vacuum states included at $\Delta E = 0$ to illustrate the roughly factor of three reduction in the QE at low excess energies that is caused by the density of vacuum states at low emitted electron momenta. Further, both our photoemission simulation and the analysis of Vecchione *et al* [17] clearly show the influence of the 300 K Boltzmann tail on the QE at excess energies below 0.25 eV, which also provides for a finite QE when $\Delta E < 0$.

Although incorporating a more realistic triangular barrier solution [30] and the physical properties of both the bulk and vacuum states, our one-step model of photoemission does not include a number of factors that can affect photocathode performance. First and foremost, the photoemission simulations do not include the matrix element describing the optical excitation of the electrons into the emitting 'virtual' states. This of course important for an *Ab initio* determination of the QE [24], but it is unlikely to affect the MTE evaluations from the simulated electron emission distributions unless the matrix element has a significant variation in momentum space for the excited virtual state. Second, the employed exact triangular barrier solution of Forbes and Deane [30] does not allow for the inclusion of the Schottky effect [15, 16, 35] in a formal manner. However, other than the lowering of the work function, the Schottky effect is not expected to alter significantly the presented simulation results, except perhaps at the highest acceleration fields where the exact shape of the potential barrier becomes important for electrons emitted by photo-assisted tunneling. Third, for the sake of brevity, the optical properties of the photocathode material, specifically the surface reflectivity and absorption coefficient for the incident light, are not included in our analysis but they could be incorporated for each individual photocathode material. The spectral properties of both will of course affect the photocathode QE by determining the total number density of excited electronic states per incident photon, but not the MTE as this is a self-normalized parameter. Fourth, the effects of chemical and surface roughness, which have been treated elsewhere [35–39], are omitted; that is, the photocathode surface is assumed to be flat and at a uniform potential. Fifth, as the presented one-step photoemission formalism assumes transverse momentum conservation in electron emission [22], the scattering of the excited virtual state electrons by phonons [40] during or just before emission into the vacuum is also not included. The strength of electron–phonon scattering is strongly material dependent and can be expected to result in an increased MTE and likely a reduced QE. Finally, and for the same reason, carrier–carrier scattering [15, 41] (e.g. inelastic electron–electron scattering) is not included in our analysis.

3. Simulation results

In the following sub-sections, we discuss the effect that the electron temperature, Fermi energy, and the surface acceleration field are expected to have, within one-step photoemission, on the spectral dependence of both the MTE and QE from planar photocathodes. The presented simulation results employ the Ag(100) exemplar of figure 2 as a template, changing a single parameter at a time to illustrate its effect on the photocathode's electron emission properties. As the QE is not explicitly evaluated from first principles, all the QE data is normalized to that at $\Delta E = 0$ for the Ag(100) photocathode in a DC gun ($\phi = 4.36$ eV, band electron effective mass $m^* = m_0$, $\varepsilon_F = 5.49$ eV, $T_{\mathrm{e}} = 300$ K, and a surface acceleration field $E_{\mathrm{acc.}} = 1$ MV m^{-1}).

3.1. Electron temperature

The effect of changing the photocathode temperature, or more specifically the temperature T_{e} of the electron distribution in the simulated isotropic Ag(100) band, is shown in figure 3. As expected, the MTE below the work function ($\Delta E < 0$) is strongly temperature dependent due to over barrier emission from the Boltzmann tail of the electron distribution (figure 3(a)). In this region just below photoemission threshold, the minimum value of the MTE is again ~25% greater than $k_{\mathrm{B}}T_{\mathrm{e}}$, primarily due to the influence of the vacuum density of states. At lower negative excess energies, photo-assisted tunneling starts to dominate the over barrier emission from the thermal tail of the electron distribution and the MTE decreases due to the strong reduction in tunneling probability with transverse momentum p_T—an effect not visible in figure 3(a). At high positive excess energies, when $\Delta E \gg k_{\mathrm{B}}T_{\mathrm{e}}$, the spectral dependence of the MTE tends to the low temperature value since the effect of the Boltzmann tail population is diminished with respect to the rest of the occupied emitting states. The low

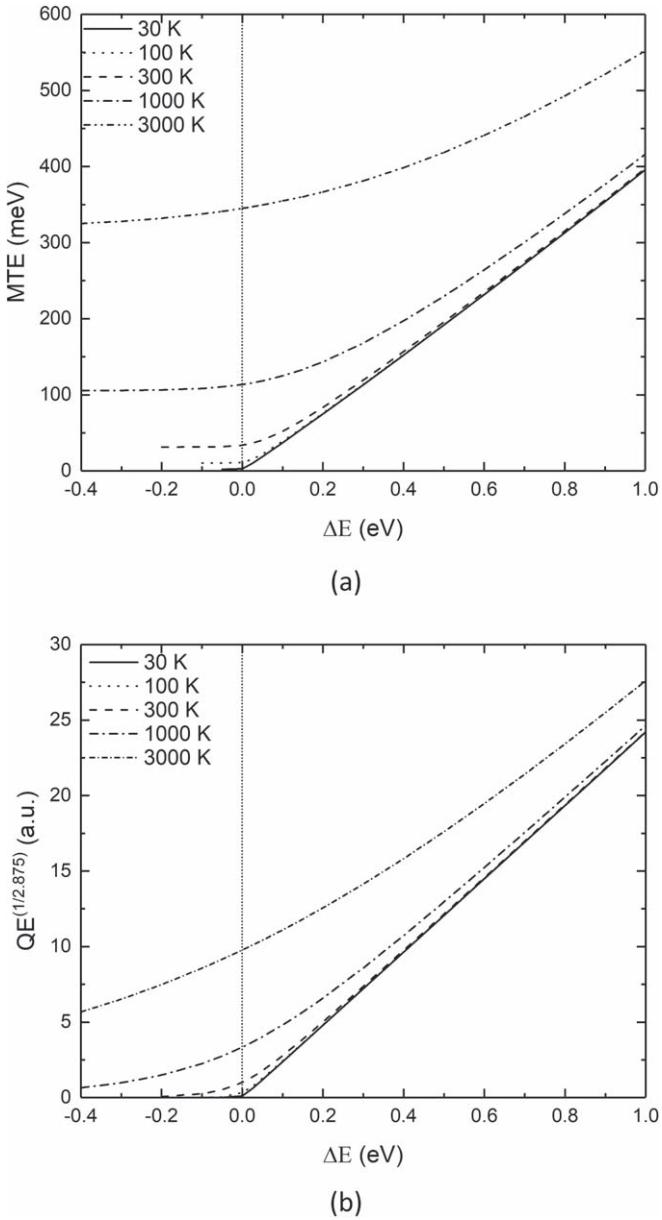

Figure 3. Emission characteristics of a Ag(100) photocathode ($\phi = 4.36$ eV, bulk electron mass $= m_0$, $\varepsilon_F = 5.49$ eV, and $E_{\text{acc.}} = 1$ MV m^{-1}) for electron temperatures T_e of 30, 100, 300, 1000, and 3000 K: (a) MTE and (b) QE$^{1/2.875}$ as a function of excess photoemission energy.

temperature linear dependence of the MTE on the excess photoemission energy is of the form $\Delta E/2.53$, which is to be compared with $\Delta E/3$ from the prior analyses [15, 17] that do not include the combined effects of the bulk and vacuum states.

For electron temperatures $T_e < 100$ K, our one-step photoemission simulation predicts that MTE values less than 10 meV should be attainable at low or negative excess energies for photocathode materials with similar parabolic band structures and $m^* \approx m_0$; for example, appropriately oriented single-crystals of Cu, Au, and the alkali group metals [42]. We also note that a recent study of cryo-cooled Cs_3Sb photocathodes illuminated at 690 nm reported a reduction of the MTE from ~43 meV at 300 K to ~12 meV at 90 K [43]. As in this case electron emission is expected to be from the Boltzmann tail of the electron distribution photo-excited into the conduction band states, the fact that both measured MTE values are greater than their corresponding thermal values of 25 and 8 meV is consistent with our predicted influence of the vacuum density of states on the MTE of electron emission. For Cs_3Sb, an additional factor is likely be the effective mass m^* and dispersion of the emitting conduction band state.

The spectral dependence of the QE at different electron temperatures T_e (figure 3(b)) also illustrates the strong influence of bulk band population in the Boltzmann tail at low and negative excess photoemission energies. Here we have plotted the normalized QE to the 0.348 (=1/2.875) power against ΔE as this power law

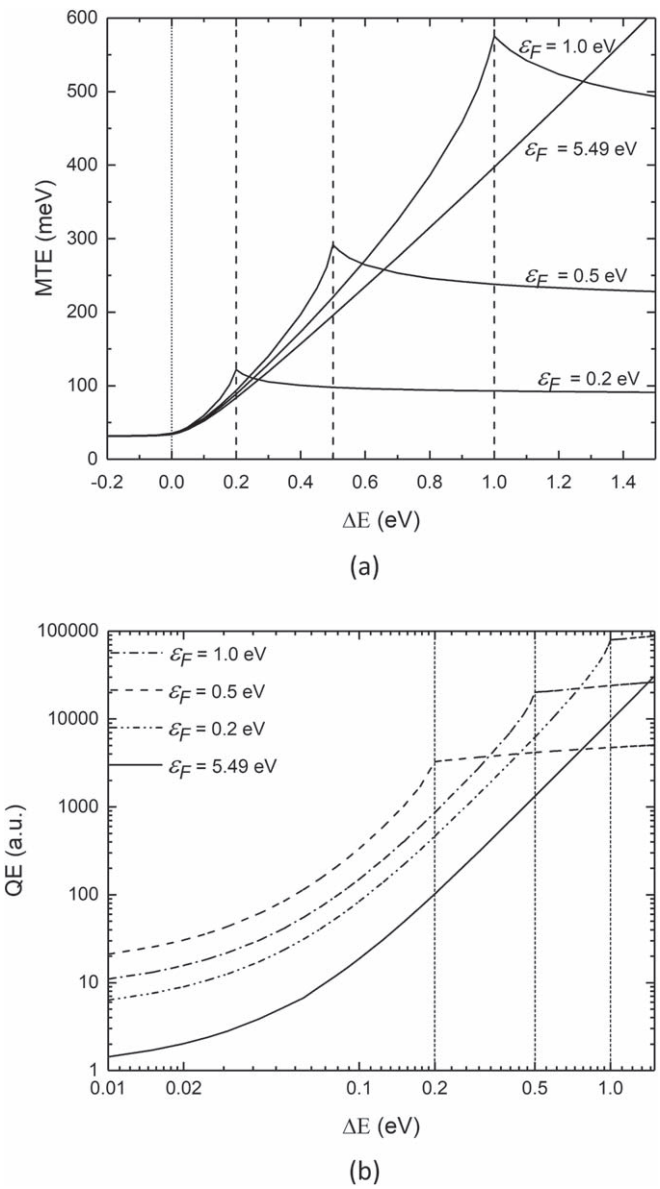

Figure 4. Simulated dependence of (a) the MTE and (b) the QE on the excess photoemission energy for Fermi energies of 0.2, 0.5, and 1.0 eV ($\phi = 4.36$ eV, bulk electron mass $= m_0$, $T_e = 300$ K, and $E_{acc.} = 1$ MV m^{-1}). The vertical dashed lines indicate were $\Delta E = \varepsilon_F$ for the three cases and the results for the Ag(100) photocathode ($\varepsilon_F = 5.49$ eV) are also shown.

dependence is the best fit to the simulation data at the lowest 30 K temperature where the Boltzmann tail population has the smallest effect. As T_e increases much beyond 300 K, where QE$^{1/2.85}$ provides the best linear dependence with ΔE (figure 2(b)), it is clear that a simple power law of the form QE $= A(\Delta E)^n$ is no longer a valid expression for excess energies below 1 eV. Nonetheless, for T_e around room temperature and below, a plot of QE$^{1/n}$ against ΔE should allow for the extraction of the photocathode work function with reasonable accuracy [44], provided that the linear fit employs measurements taken for $\Delta E > 10k_B T_e$. As will be shown below, such a power law scaling for the QE only exists if the band Fermi energy ε_F is much greater than the excess photoemission energy ΔE.

3.2. Fermi energy

As the Fermi energy defines the energy of the last electron in the bulk band as $T_e \rightarrow 0$, the emission properties of a solid-state photocathode are expected to be affected when ΔE is of the order of or greater than ε_F. The results of a one-step photoemission simulation for Fermi energy values of 0.2, 0.5 and 1 eV, depicted in figure 4, show that this is indeed the case. In all cases, the dependence of the MTE on ΔE (figure 4(a)) is similar to that in figure 2(a) for $\varepsilon_F = 5.49$ eV (dotted–dashed line) at low excess energies, but displays a distinct 'cusp' when $\Delta E = \varepsilon_F$ (vertical dashed lines). At this critical value of the excess energy, all the excited bulk band electronic states with positive p_z (in the direction of emission) are 'resonantly' matched in momentum and energy to the vacuum states

leading to an increased transmission through the barrier at all p_T and hence a larger MTE. As ΔE increases beyond ε_F, the MTE levels off to a slightly lower and relatively constant value as the barrier transmission for the electrons excited from the bulk band moves off the $\Delta E = \varepsilon_F$ resonance and becomes less dependent on ΔE. This interpretation is supported by the spectral dependence of the QE displayed in figure 4(b) which shows a clear trend discontinuity at $\Delta E = \varepsilon_F$, just when all the band states with positive p_z can emit. At higher ΔE, the barrier transmission does increase [30], but no new states are available leading to a slower increase in QE with ΔE.

Also evident from the log–log plot in figure 4(b) is that the QE no longer follows a simple power law dependence with excess energy, QE $= A(\Delta E)^n$ for $\Delta E > 10k_{\mathrm{B}}T_{\mathrm{e}}$, when one-step photoemission is from a bulk band with a low Fermi energy. This must be the case since significant changes in the number density of available photo-emitting states occur as ΔE increases for excess energies less than, but of the order of, the Fermi energy. As a result, extraction of a value for the work function using measured QE data may prove difficult without a functional photoemission model in cases where ε_F is in the range of $10 - 100k_{\mathrm{B}}T_{\mathrm{e}}$. In addition, we note that the one-step photoemission QE from the bulk band near threshold increases as the Fermi energy decreases—all the QE data being normalized to that at $\Delta E = 0$ for $\varepsilon_F = 5.49$ eV and $T_{\mathrm{e}} = 300$ K (figure 2(b)). This is a direct result of increased barrier transmission when the longitudinal momentum p_z of an excited emitting state is closer to the momentum of the emitted electron p_{z0} from that bulk state.

3.3. Surface acceleration field

Although the Schottky effect is not included in our one-step photoemission simulation, it is nonetheless informative to examine the predicted effect of the surface acceleration field E_{acc} on both the MTE and QE within the exact triangular barrier solution [30]. Figure 5(a) shows the dependence of the MTE on the acceleration field for selected near threshold excess photoemission energies of −0.1, −0.05, 0. 0.05, and 0.1 eV. At positive values of ΔE, the MTE is fairly independent of E_{acc} as above barrier photoemission dominates. Closer to photoemission threshold there are more significant effects. Most notably, the MTE is reduced for $\Delta E < 0$ as the applied field is increased, reaching a minimum value below the $k_{\mathrm{B}}T_{\mathrm{e}} = 25$ meV thermal energy for surface fields between 40 and 80 MV m^{-1} when $\Delta E < -0.05$ eV. This lower than expected MTE value is caused by the increased contribution at higher E_{acc} of photo-assisted tunneling to the transverse momentum distribution of the emitted electrons. This contribution has a MTE lower than 25 meV for fields less than about 80 MV m^{-1} due to the rapid drop in barrier tunneling transmission probability as p_T increases for an electron at a given bulk band energy. At higher fields, the triangular barrier becomes sufficiently narrow to increase the tunneling transmission probability at larger p_T so that the MTE again increases somewhat for $\Delta E < 0$. As a result, a minimum in the MTE develops below the photoemission threshold—an effect that may not be observable experimentally since the Schottky effect is not included in this photoemission simulation.

The effect of E_{acc} on the QE follows expected trends and is displayed in figure 5(b) for the same selected near threshold excess photoemission energies of −0.1, −0.05, 0. 0.05, and 0.1 eV. At low surface field strengths, where above barrier photoemission dominates, the QE slowly decreases with increasing E_{acc} due to the initial $E_{\mathrm{acc}}^{-1/3}$ dependence of the transmission coefficient for the triangular barrier (equation (3)). At field strengths greater than 20 MV m^{-1}, the contribution from photo-assisted tunneling increases and this eventually reverses the initial trend—the point of reversal being at lower values of E_{acc} for lower values of ΔE since the QE of above barrier photoemission (due to the photo-excited Boltzmann tail of the electron distribution) falls rapidly with decreasing ΔE below the photoemission threshold. Aside from the increased tunneling probability at higher acceleration fields, we note that a higher density of recipient vacuum states is also available at larger E_{acc} since equation (5*b*) states that the longitudinal momentum of the electron emerging into the vacuum from the barrier increases with the cubic root of E_{acc}.

4. Summary

A one-step photoemission analysis is presented that employs the exact triangular barrier transmission solution of Forbes and Deane [30] to evaluate the MTE and QE (in relative terms) associated with the transition from the emitting bulk band states to the recipient vacuum states. The inclusion of both the local density of the virtual excited band states and the physical characteristics of the vacuum states is shown to have a significant effect on both the MTE of the electron distribution emitted from photocathodes and the QE of photoemission. For an electron-like (positive dispersion) bulk emission band, the vacuum density of states is shown to limit the minimum MTE attainable at low (and negative) excess energies to values about 25% greater than $k_{\mathrm{B}}T_{\mathrm{e}}$ when $\Delta E > -10k_{\mathrm{B}}T_{\mathrm{e}}$. Similarly, for positive excess photoemission energies, the combined physical characteristics of both the emitting band and the vacuum contribute to MTE values about 20% greater than that of the poly-logarithmic functional form of equation (6) [17] when $\Delta E \ll \varepsilon_F$. For the QE, the one-step photoemission

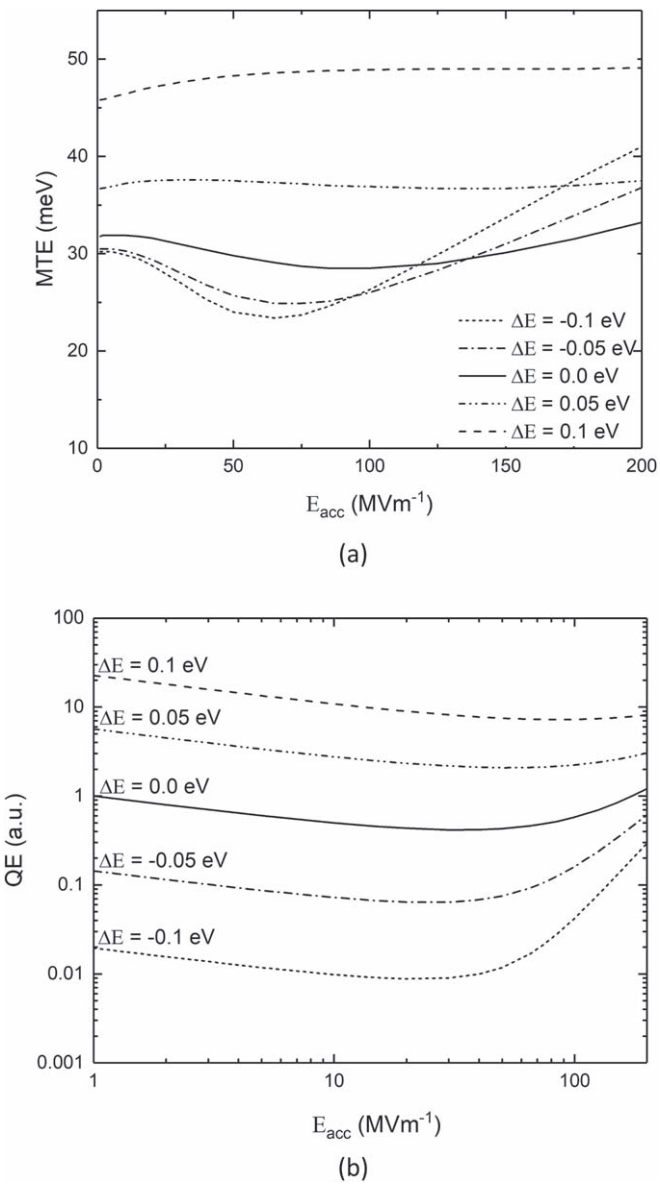

Figure 5. Simulated emission properties of a Ag(100) photocathode ($\phi = 4.36$ eV, bulk electron mass $= m_0$, $\varepsilon_F = 5.49$ eV, and $T_e = 300$ K) as a function of applied surface acceleration field for near threshold excess photoemission energies of −0.1, −0.05, 0. 0.05, and 0.1 eV: (a) MTE and (b) normalized QE.

analysis indicates that the same effects will alter the quadratic power law dependence of the QE on excess energy predicted by equation (7) [17] for $\Delta E > 10k_BT_e$ to a power law dependence closer to cubic [44]. As these simulation results represent a significant departure from prior theoretical formalisms of photoemission [15, 17, 19, 33, 34], they will need to be verified by experiment, ideally using single-crystals of commonly used photocathode materials; for example, Cu(100) as there is a single electron-like emission band in this case. Similarly, the predicted variation of the MTE and QE with excess photoemission energy when $\Delta E \sim \varepsilon_F$ (figure 4) for the simulated first Brillouin zone Γ point emitter will also require experimental verification.

The one-step photoemission analysis also indicates that the MTE of the emitted electron distribution could decrease by 20%–30% and the QE increase by about a factor of 2 near (and below) the photoemission threshold when the surface acceleration field is around 50 MV m^{-1} (figure 5), although the Schottky effect [15, 16, 35] is not taken into account. However, since the QE is usually quite low ($\sim 10^{-7}$ or less) when $\Delta E \approx 0$, large incident laser powers are likely to be required to generate sufficient electrons for may practical requirements. For short electron pulse generation with ultrafast ps and sub-ps laser pulses, significant laser-induced heating of the electron distribution in the photocathode material can then result [45], so that the anticipated reduction in MTE will likely be more than offset by the resultant increase in T_e (see figure 3).

Although the presented photoemission simulation results have only employed an emitting band with spherical symmetry and an electron mass equal to the free electron mass, extension of the analysis to more

realistic bulk bands encountered in photocathode materials appears quite possible. In particular, extension to parabolic electron-like bulk bands that possess cylindrical symmetry about the emission direction, but are characterized by a longitudinal effective electron mass different from that in the transverse direction, is straightforward. Inversion of the dispersion for hole-like bands, which may have different spectral dependences for the MTE and QE since their density of states increases (rather than decreases) with increasing ΔE, should also be possible. In principle, a direct connection could be made with the actual $E(\mathbf{p})$ dispersion of the emitting band (s) in real photocathode materials using density functional theory based band structure calculations. It is further noteworthy that the presented analysis may also be employed to simulate the final emission step in three-step photocathode emitters, such as negative electron affinity photocathodes, once the temporal dynamics of the carrier distribution after photo-excitation are known, since figure 4 already shows results for $\Delta E > \varepsilon_F$.

Acknowledgments

The authors gratefully acknowledge support for this work from the National Science Foundation (Award no. NSF-1535279).

References

[1] Chapman H N *et al* 2006 Femtosecond diffractive imaging with a soft-x-ray free-electron laser *Nat. Phys.* **2** 839–43
[2] Fritz D M *et al* 2007 Ultrafast bond softening in bismuth: mapping a solid's interatomic potential with x-rays *Science* **315** 633
[3] Sciaini G, Harb M, Kruglik S G, Payer T, Hebeisen C T, Meyer zu Heringdorf F-J, Yamaguchi M, Horn-von Hoegen M, Ernstorfer R and Miller R J D 2009 Electronic acceleration of atomic motions and disordering in bismuth *Nature* **458** 56
[4] Miller R J D 2014 Mapping atomic motions with ultrabright electrons: the chemists' gedanken experiment enters the lab frame *Annu. Rev. Phys. Chem.* **65** 583–604
[5] Hastings J B, Rudakov F M, Dowell D H, Schmerge J F, Cardoza J D, Castro J M, Gierman S M, Loos H and Weber P M 2006 Ultrafast time-resolved electron diffraction with megavolt electron beams *Appl. Phys. Lett.* **89** 184109
[6] Musumeci P, Moody J T, Scoby C M, Gutiernez M S, Bender H A and Wilcox N S 2010 High quality single shot diffraction patterns using megaelectron volt electron beams from a radio frequency photoinjetcor *Rev. Sci. Instrum.* **81** 013306
[7] LaGrange T *et al* 2006 Single-shot dynamic transmission electron microscopy *Appl. Phys. Lett.* **89** 044105
[8] Yang J, Yoshida Y and Shibata H 2015 Femtosecond time-resolved electron microscopy *Electron. Commun. Japan.* **98 50** translated from Denki Gakkai Ronbunshi Yang J, Yoshida Y and Shibata H 2014 *Electron. Commun. Japan.* **134-C** 515–20
[9] Li R K and Musumeci P 2014 Single-shot MeV transmission electron microscopy with picosecond temporal resolution *Phys. Rev. Appl.* **2** 024003
[10] Bazarov I V, Dunham B M and Sinclair C K 2009 Maximum achievable beam brightness from photoinjectors *Phys. Rev. Lett.* **102** 104801
[11] Gulliford C *et al* 2013 Demonstration of low emittance in the Cornell energy recovery linac injector prototype *Phys. Rev. Spec. Top. Accel. Beams* **16** 073401
[12] Xie M Design optimization for an x-ray free electron laser driven by SLAC linac *Proc. 1995 Particle Accelerator Conf.* (Dallas, TX: IEEE) pp 183–5 95CH35843
[13] Huang Z and Kim K J 2007 Review of x-ray free-electron laser theory *Phys. Rev. Spec. Top. Accel. Beams* **10** 034801
[14] van Oudheusen T, de Jong E F, van der Geer S B, Op t Root W P E M, Luiten O J and Siwick B J 2007 Electron source concept for single-shot sub-100fs electron diffraction in the 100 keV range *J. Appl. Phys.* **102** 093501
[15] Dowell D and Schmerge J 2009 Quantum efficiency and thermal emittance of metal photocathodes *Phys. Rev. Spec. Top. Accel. Beams* **12** 074201
[16] Jensen K L, O'Shea P G, Feldman D W and Shaw J L 2010 Emittance of a field emission electron source *J. Appl. Phys.* **107** 014903
[17] Vecchione T, Dowell D, Wan W, Feng J and Padmore H A 2013 *35th Int. Free-Electron Laser Conf. (New York, NY)* 424–6
[18] Rickman B L, Berger J A, Nicholls A W and Schroeder W A 2013 Intrinsic electron beam emittance from metal photocathodes: the effect of the electron effective mass *Phys. Rev. Lett.* **111** 237401
Rickman B L, Berger J A, Nicholls A W and Schroeder W A 2014 Erratum: Intrinsic Electron beam emittance from metal photocathodes: the effect of the electron effective mass [Phys. Rev. Lett. **111**, 237401 (2013)] *Phys. Rev. Lett.* **113** 239904
[19] Feng J, Nasiatka J, Wan W, Karkare S, Smedley J and Padmore H A 2015 Thermal limit to the intrinsic emittance from metal photocathodes *Appl. Phys. Lett.* **107** 134101
[20] Li T, Rickman B L and Schroeder W A 2015 Emission properties of body-centered cubic elemental metal photocathodes *J. Appl. Phys.* **117** 134901
[21] Li T, Rickman B L and Schroeder W A 2015 Density functional theory analysis of hexagonal close-packed elemental metal photocathodes *Phys. Rev. Spec. Top. Accel. Beams* **18** 073401
[22] Himpsel F J 1983 Angle-resolved measurements of the photoemission of electrons in the study of solids *Adv. Phys.* **32** 1–51
[23] See for example Derry G N, Kern M E and Worth E H 2015 Recommended values of clean metal work functions *J. Vac. Sci. Technol.* A **33** 060801
[24] Karkare S, Feng J, Chen X, Wan W, Palomares F J, Chiang T-C and Padmore H A 2017 Reduction of intrinsic electron emittance from photocathodes using ordered crystalline surfaces *Phys. Rev. Lett.* **118** 164802
[25] Adhikari G D and Schroeder W A 2017 Spectral intrinsic emittance measuremnts of Mo(001) and PbTe(111) photocathodes *European Workshop on Photocathodes for Particle Accelerator Applications (EWPAA)* 2017 (Berlin, Germany: Helmholtz-Zentrum)
[26] Karkare S, Padmore H A, Adhikari G D and Schroeder W A 2018 Intrinsic emittance of single crystal cathodes *International Particle Accelerator Conference (IPAC) (Vancouver, British Columbia, Canada, 29April–4 May 2018)* (https://doi.org/10.18429/JACoW-IPAC2018-THPMF081)
[27] Galdi A *et al* 2018 Barium tin oxide photocathodes: first measurements and future perspectives *Int. Particle Accelerator Conf. (IPAC) (Vancouver, British Columbia, Canada, 29 April–4 May 2018)* (https://doi.org/10.18429/JACoW-IPAC2018-TUPML027)

[28] Karkare S, Wan W, Feng J, Chiang T-C and Padmore H A 2017 One-step model of photoemission from single-crystal surfaces *Phys. Rev.* B **95** 075439
[29] Mahan G D 1970 Theory of photoemission in simple metals *Phys. Rev.* B **2** 4334
[30] Forbes R G and Deane J H B 2011 Transmission coefficients for the exact triangular barrier: an exact analytical theory that can replace Fowler & Nordheim's1928 theory *Proc. R. Soc.* A **467** 2927
[31] See, for example Pankove J I 1975 *Optical Processes in Semiconductors* (New York: Dover Publications Inc.)
[32] See, for example Johnson P B and Christy R W 1972 Optical constants of the noble metals *Phys. Rev.* B **6** 4370–9
[33] Fowler R H 1931 The analysis of photoelectric sensitivity curves for clean metals at various temperatures *Phys. Rev.* **38** 45–56
[34] DuBridge L A 1933 Theory of the energy distribution of photo-electrons *Phys. Rev.* **43** 727–41
[35] Qian H J, Li C, Du Y C, Yan L X, Hua J F, Huang W H and Tang C X 2012 Experimental investigation of thermal emittance components of copper photocathode *Phys. Rev. Spec. Top. Accel. Beams* **15** 040102
[36] Karkare S and Bazarov I 2015 Effects of surface non-uniformities on the mean transverse energy from photocathodes *Phys. Rev. Appl.* **4** 024015
[37] Bradley D J, Allenson M B and Holeman B R 1977 The transverse energy of electrons emitted from GaAs photocathodes *J. Phys. D: Appl. Phys.* **10** 111
[38] Karkare S and Bazarov I 2011 Effect of nanoscale surface roughness on transverse energy spread from GaAs photocathodes *Appl. Phys. Lett.* **98** 094104
[39] Zhang Z and Tang C 2015 Analytical study of emittance growth caused by roughness of a metallic photocathode *Phys. Rev. Spec. Top. Accel. Beams* **18** 053401
[40] Nangoi J K, Arias T A, Karkare S, Padmore H A and Schroeder W A 2018 The role of electron–phonon scattering in transverse momentum conservation in PbTe(111) photocathodes *Int. Particle Accelerator Conf. (IPAC) (Vancouver, British Columbia, Canada, 29 April–4 May 2018)* (https://doi.org/10.18429/JACoW-IPAC2018-TUPMF065)
[41] Wooten F, Hernandez J P and Spicer W E 1973 Photoemission and electron scattering in Cs_3Bi and Cs_3Sb *J. Appl. Phys.* **44** 1112
[42] Weaire D 1967 Band effective masses for nineteen elements *Proc. Phys. Soc.* **92** 956–61
[43] Cultrera L 2017 Photoemission research at Cornell University: recent advances and future perspectives *European Workshop on Photocathodes for Particle Accelerator Applications (EWPAA) 2017* September 20–22(Berlin, Germany: Helmholtz-Zentrum)
[44] Gobeli G W and Allen F G 1965 Photoelectric properties of cleaved GaAs, GaSb, InAs, and InSb surfaces; comparison with Si and Ge *Phys. Rev.* **137** A245
[45] Chen Y J K, Tzou D Y and Beraun J E 2006 A semiclassical two-temperature model for ultrafast laser heating *Int. J. Heat Mass Transfer* **49** 307–16